

Black silicon UV photodiodes achieve >130% external quantum efficiency

M. Garin,^{1,2,3} J. Heinonen,^{1,4} L. Werner⁵, T. P. Pasanen,¹ V. Vähänissi,¹ A. Haarahiltunen,⁴ M. Juntunen,⁴ H. Savin,^{1}*

¹ Department of Micro and Nanosciences, Aalto University, Tietotie 3, Espoo 02150

² Department of Engineering, Universitat de Vic – Universitat Central de Catalunya, c/ de la Laura 13, 08500 Vic, Spain.

³ Univ. Politècnica de Catalunya, Gran Capità s/n, 08034 Barcelona, Spain

⁴ EIFys inc, Tekniikantie 12, Espoo 02150

⁵ Physikalisch-Technische Bundesanstalt, Abbestr. 2-12, 10587 Berlin, Germany

* hele.savin@aalto.fi

ABSTRACT

At present ultraviolet sensors are utilized in numerous fields ranging from various spectroscopy applications via biotechnical innovations to industrial process control. Despite of this, the performance of current UV sensors is surprisingly poor. Here, we break the theoretical Shockley-Queisser limit and demonstrate a device with a certified external quantum efficiency (EQE) above 130% in UV range without external amplification. The record high performance is obtained using a nanostructured silicon photodiode with self-induced junction. We show that the high efficiency is based on effective utilization of multiple carrier generation by impact ionization taking place in the nanostructures. While the results can readily have a significant impact on the UV-sensor industry, the underlying technological concept can be applied to other semiconductor materials, thereby extending above unity response to longer wavelengths.

INTRODUCTION

Ultraviolet (UV) sensors are currently being utilized in a wide range of applications, including spectroscopy, imaging, index monitoring, flame detection, water purification and biotechnology—just to name a few. [1, 2, 3, 4, 5, 6] Furthermore, the corresponding sensor market is expected to grow at a compound annual growth rate of about 30%. [7] Therefore, it is quite surprising that the current semiconductor sensors available in the market suffer from relatively poor UV response, the best sensitivities falling well below 80% at 200-300 nm [8, 9]. All the UV applications would greatly benefit from better response, therefore, there is a strong interest to seek for alternative technologies that could provide higher efficiencies in this challenging wavelength regime.

Traditionally, the so-called Shockley-Queisser (SQ) limit [10] has been considered as the maximum theoretical efficiency for single-junction photovoltaic devices at zero bias. SQ assumes, among other things, that one photon can generate at maximum one electron-hole pair (e-h pair). In the UV regime this means that even though hot carriers are generated by high-energy photons, their excess energy is quickly lost as thermal energy. However, nowadays it is well known that this limit can be overcome by the so-called carrier multiplication process, *i.e.* the phenomenon in which the excess energy of hot carriers is utilized to produce further electron-hole pairs by impact ionization. This type of carrier multiplication requires the photon energy to be at least two times the bandgap ($E_{ph} > 2 \times E_g$) and its probability increases linearly with photon energy, leading in silicon to an average pair-creation energy of about 3.6 eV [11, 12, 13]. Indeed, several examples of internal quantum yield (*i.e.* number of e-h pairs generated by a single photon) exceeding one can be found in the literature for both silicon and germanium [14, 15, 16, 17, 18, 19, 20, 21, 22, 23, 24, 25].

While carrier multiplication via high-energy photons would seem an ideal phenomenon to increase the sensitivity of the semiconductor sensors, to date it has not been successfully demonstrated in real photovoltaic devices. Despite multiple efforts and promising results in internal quantum yields, the external quantum yields that determine the real device performance, have remained rather modest. As surprising as this might seem, there are two fundamental technological obstacles to be encountered when considering the current state-of-the-art silicon UV photodiodes. Firstly, the reflectance losses are typically high in the UV range due to the high refractive index

of silicon, making it challenging to reach high external quantum yields without advanced antireflection techniques. Secondly, high-energy photons are absorbed in the vicinity of the surface and, therefore, the photogenerated charge carriers are extremely sensitive to surface recombination. Consequently, technological improvements in the reflection via micro- and/or nanotexturing are usually counterbalanced by an increase of surface recombination, resulting in spectral responses with external quantum yields far from one. Nonetheless, the recently proposed broadband induced-junction black silicon photodiode [26] seems a promising candidate for overcoming the aforementioned obstacles. It consists of a non-reflecting nanostructure combined with efficient surface passivation and junction formation by a highly-charged and conformal alumina thin film. The preliminary results published in that work have yielded external quantum yield close to 100%. However, the performance of the photodiode in the UV range (below 300nm) has not been confirmed nor the physical phenomena in the induced junction inside nanostructures are known, especially when the UV photons are absorbed only within 10 nm from the surface. Carrier multiplication is likely to take place but, due to the presence of nanostructures, quantum confinement or related phenomena cannot be excluded without further studies.

Here we study the applicability of the induced-junction black silicon photodiodes for UV detection. First, we accurately determine the external quantum yield of the diodes and verify the results by independent measurements at PTB (Physikalisch-Technische Bundesanstalt, Berlin) with a maximum relative standard uncertainty of 0.4 %. Special emphasis is put on the UV range ($\lambda=200\text{-}350\text{ nm}$) where we show that extremely high response, more than 130%, can be achieved at zero bias. This clearly exceeds all previously reported values in this wavelength range. To gain a more in-depth understanding of the physical phenomena, we first analyze the electric field and electrostatic potential distributions inside the nanoscale needles using Silvaco Atlas simulations. Then we examine the internal quantum yield of the corresponding induced junction photodiode with planar surface. Finally, we compare the features in the internal quantum yield spectra to those reported earlier in devices known to possess carrier multiplication. The results allow us to determine the relevant physical mechanisms leading to an external quantum yield $>130\%$.

RESULTS & DISCUSSION

Figure 1 shows the external and internal quantum efficiencies (EQE, IQE) of the black silicon induced-junction photodiode (see inset for schematic device cross-section) measured at zero bias in the visible and UV range extending down to 200 nm. The EQE values exceed 100% at wavelengths shorter than, 310 nm, approximately, and reach values even larger than 130 % close to 200 nm. Such high values measured at UV exceed by far all the EQE values reported in literature. In addition, the IQE and the EQE of the device are nearly identical, which is related to the very low reflectance achieved with black silicon (2% av. in the UV). This is a rather unique characteristic clearly demonstrating the superior optical and electronic behavior of the device.

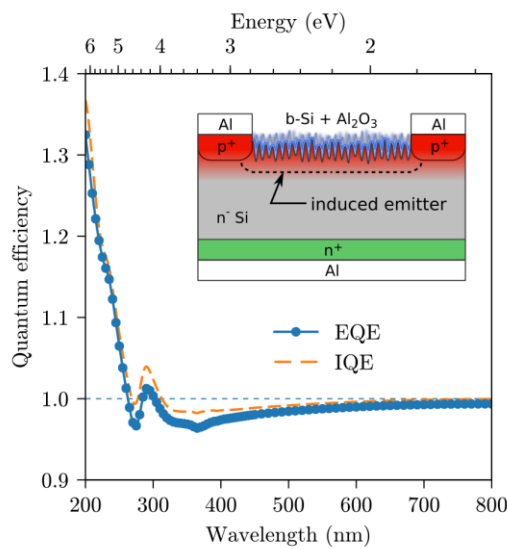


Fig. 1. External (blue circles) and internal (yellow dashed) quantum efficiency of the induced-junction black-silicon photodiode measured at zero bias. The inset shows schematically the structure of the device.

The results demonstrate that black-silicon induced-junction photodiode structure is particularly sensitive to UV radiation, which is absorbed in the first few nanometers of the device. The excellent sensitivity can be explained as follows: *i)* the induced junction avoids harmful Auger recombination near the front surface, *ii)* a strong electric field at the surface ensures immediate collection of the photogenerated carriers, *iii)* nano-texturing efficiently suppresses reflection losses in the UV, and *iv)* surface recombination losses can be minimized due to excellent passivation achieved with Al_2O_3 . These characteristics alone ensure both collection efficiencies and EQE values close to 100% even without the presence of carrier multiplication or other alternative generation processes. However, in reality at high photon energies carrier multiplication is likely to take place. Therefore, this structure is close to an ideal platform to observe, explore and utilize carrier multiplication.

While it is known that the charge collection efficiency is high in the above device, it is not known whether the presence of ALD coated nanostructures affects the probability of carrier multiplication. In other words, when a photon is absorbed in silicon, whether the black silicon induced junction will boost carrier multiplication in comparison to its planar counterpart with doped pn-junction. A possible mechanism for carrier multiplication enhancement could be related to the high charge density present in the Al_2O_3 , which is typically in the range of $1\text{--}5 \times 10^{12} \text{ cm}^{-2}$. [27, 28]. The charge induces an intense electric field, which is possibly concentrated within the nanostructure, and which should have its maximum near the surface right where the impinging UV photons are absorbed. This could be considered somewhat analogous to avalanche photodiodes, in which a high electric field is generated by an external bias voltage. However, here the surface field would most probably assist carrier multiplication only on hot enough carriers resulting from UV photons. To study whether such an effect might be feasible, we show in Figure 2 both the simulated E -field distribution and the electrostatic potential for a single cylindrical-symmetric black silicon nano-needle in thermal equilibrium. The simulations were performed considering a bulk resistivity of $10 \text{ k}\Omega\cdot\text{cm}$ (n-type) and an Al_2O_3 fixed charge of $Q_f = 2.5 \times 10^{12} \text{ cm}^{-2}$. The simulations reveal that there is no particular increase in the maximum E -field intensity inside the nano-needle, even at the apex of the nanostructure. The maximum intensity value stays around 300 kV/cm , which is in the same order as expected for a planar surface with the same level of fixed charge. In general, electric fields in the order of 10^6 V/cm are required to cause a noticeable generation rate by impact ionization in silicon. [29] Although close, the electric field induced by the Al_2O_3 layer is not high enough to cause impact ionization, especially when taking into account that the field decreases rapidly in just a few nanometers below the surface.

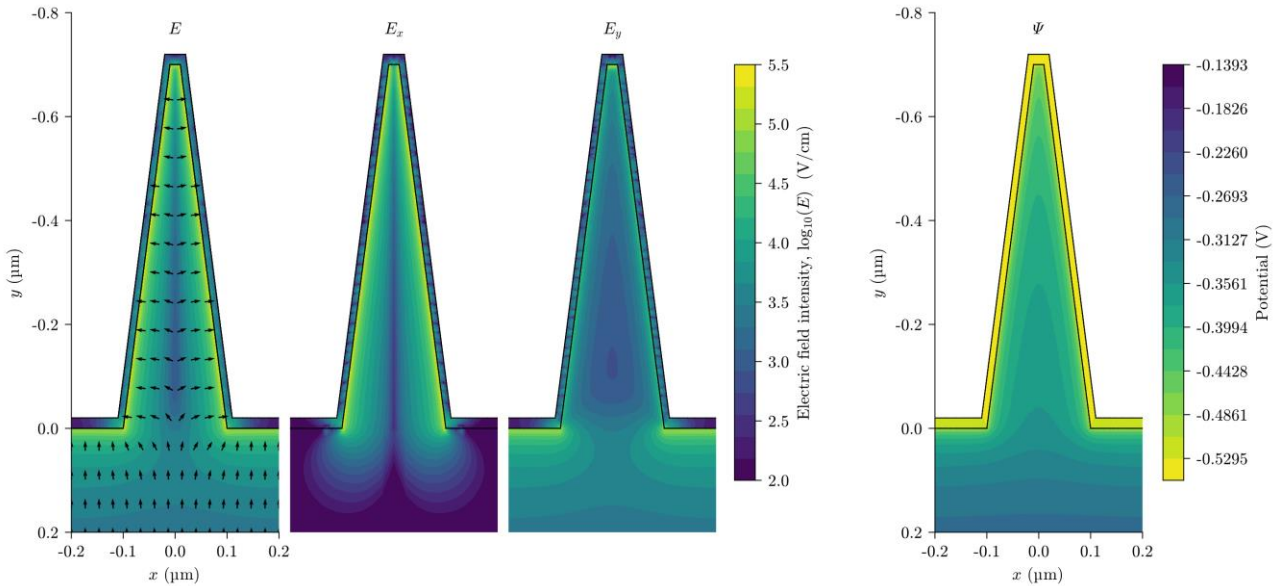


Fig. 2. Simulated electrical field distribution (left) and electrostatic potential (right) in a single black silicon nano-needle.

Although simulations discard any electric field hotspots, they reveal an interesting electric field distribution inside black silicon. Due to the cylindrical/conical shape of the nano-needles, the electric field inside the needle is nearly completely confined into the x direction. Obviously, E_x neutralizes around the symmetry axis of the needle, but in average E_y stays much lower than E_x throughout the needle volume. On the contrary, E_y noticeably increases at the bottom of the nanostructure resulting in a local maximum, while E_x quickly vanishes outside the needle. Both E_y and E_x have low intensity around the symmetry axis of the Si needle due to geometric constraints. Despite of that, the density of holes required to equal the charge Q_f needs to be high in the whole black Si volume

due to both the small dimensions and the large surface-to-volume ratio of the nano-structure. This imposes a high electrostatic potential through the whole volume, including the base of the needle, which then requires a sudden electric field increase right at the bottom of the needles. In a sense, it can be understood as if the y -component of the electric field is shifted down to the bottom of the needle. This particular electrostatic configuration helps masking the nanostructure from the bulk perspective, as the electrostatic potential below the nanostructure quickly flattens at a distance of around 100 nm below the nano-structures.

It is worth to emphasize that the simultaneous combination of low electric field (E) and high electrostatic potential (Ψ) inside the nanostructure is extremely unusual. In a standard planar device, the presence of E -field is always related to the existence of a space-charge-region (SCR) and, conversely, the lack of E -field is related to a homogeneously doped neutral region outside the SCR, usually the bulk. In other words, the electrostatic configuration along the core of the black-silicon nano-needles is analogous to a homogeneously doped p -type region with an equivalent doping density defined by the hole concentration present at the symmetry axis. Notice that the steeper the sidewalls of the needles, the more pronounced this effect would be. Finally, in case of vertical cylinders, E_y becomes completely negligible throughout the needle volume. The smaller the dimensions of the nanostructure, the higher the equivalent doping would need to be, since the electric dipole at the needle surface becomes confined into a smaller dimension requiring higher induced hole density. Assuming that no other effects arise, this nanoscale “virtual doping” becomes particularly notorious when dimensions are in the order of 10 nm and below, eventually inducing higher Ψ values than expected in the planar counterpart but without increasing the field at the surface. Subsequently, charge carriers generated inside the needles are quickly pushed toward the symmetry axis but, due to the absence of E_y -field, their vertical transport is limited by diffusion. The E_y field collects the charge carriers only when they reach the bottom of the nanostructures. Nevertheless, the formation of an induced junction in a nanostructured surface deserves further research in order to fully understand its consequences and dependence on different nanotexture dimensions and geometries. As far as we are concerned in this work, however, the above behavior cannot explain the observed above unity EQE values.

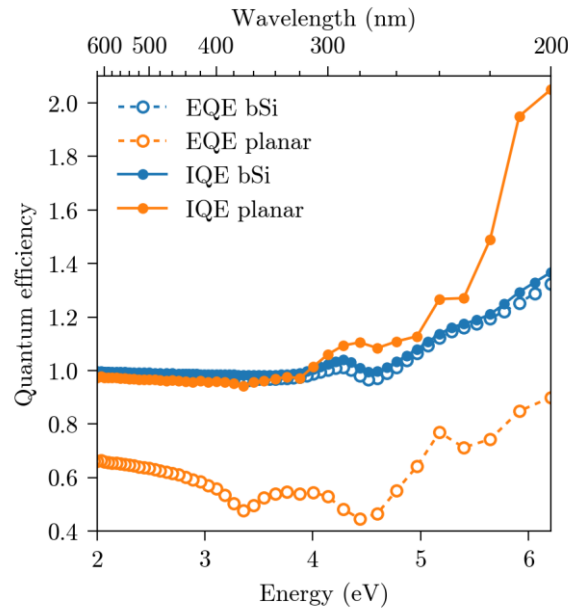


Figure 3: Comparison of both EQE (open symbols) and IQE (filled symbols) of two similar induced-junction photodiodes, one with black silicon texturing (blue circular) and another with a polished surface (orange circles).

The above simulations strongly suggested that the charged thin film on the nanostructures does not boost carrier multiplication. The next step, therefore, is to compare the measured quantum yield to corresponding planar junction. This should allow us to differentiate between the impact of the nanostructure and the induced junction. Figure 3 shows the IQE and EQE of planar and black silicon induced-junction photodiodes, having identical structures besides the surface texture. Somewhat surprisingly, the IQE of the planar photodiode clearly outperforms the black silicon photodiode, reaching IQE values above 200% at a wavelength of 200 nm. For energies above ~ 3.8 eV carrier multiplication becomes clearly visible. For higher energies, the phenomenon increases significantly as a function of photon energy, as predicted by theory. The fact that the phenomenon is clearly more pronounced in planar photodiodes further supports that we can discard any nanoscale-related effects

related to black silicon. Furthermore, we can conclude that the effective carrier recombination is higher in black silicon. It is likely that there is a higher amount of recombination sites present in b-Si (reactive ion etching induced damage, larger surface area, exposed crystal planes with varying orientation). However, as the electric field is quite small in the middle of the needles (Fig.2), the carriers need to diffuse a relatively long distance before being collected which may also increase recombination. This leads to the possibility that by reducing the aspect ratio without compromising the reflectance, the performance of black silicon photodiodes could be even higher. Obviously, other considerations, such as the enlarged effective surface and a greater density of states in the textured surface, need to be factored in during the optimization.

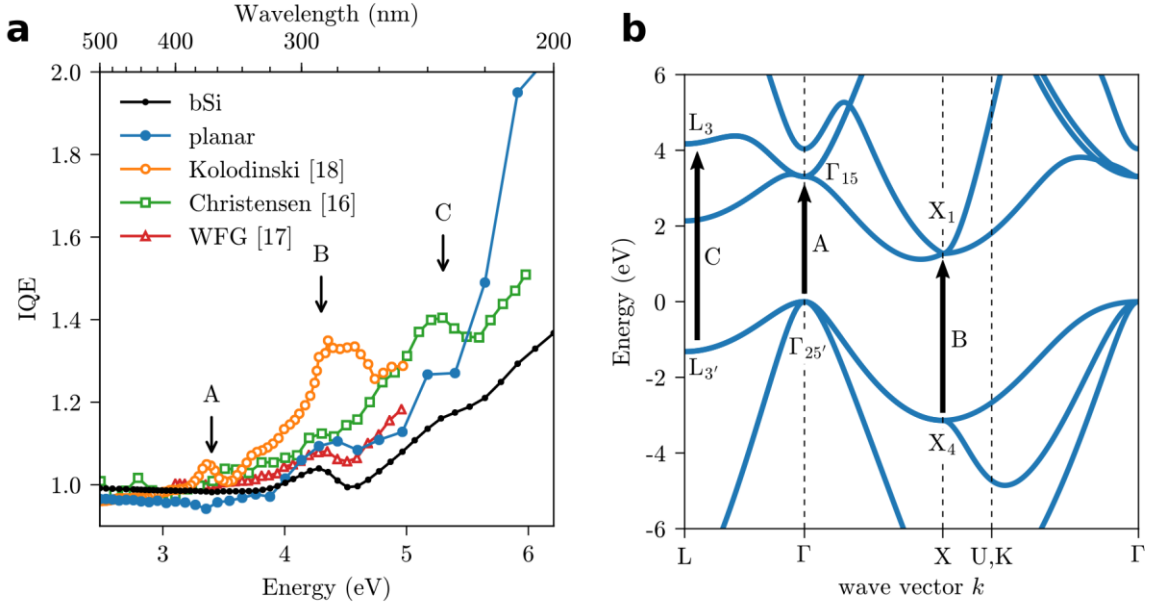


Fig. 4. **a** Comparison of the IQE reported for different silicon photodetectors with untextured surface, including this work. **b** Schematic of the band diagram for silicon.

Further insight on the physical nature of carrier multiplication in our photodiodes can be achieved through carefully inspecting the features of the IQE spectra in the UV range. Figure 4 shows the details of the IQE shapes in both black silicon and planar induced-junction diodes in comparison to previously published diodes [16, 17, 18] that possess high IQE values, above one, due to carrier multiplication. All the curves show similar spectral features that can be related to characteristics in the band structure of silicon (see Figure 4 b). It should be pointed out that carrier multiplication is particularly sensitive to the band structure in this energy range. The most prominent features in the IQE curves are the ones labelled B and C. Feature B, present at all curves at around 4.3 eV, can be associated to impact ionization by holes [18]. It corresponds to the transition X_4 - X_1 , which generates hot holes that would be responsible for the carrier generation by impact ionization. The spectral feature C, at around 5.3 eV, is likely related to the direct transition L_3 - $L_{3'}$. Interestingly, feature A is non-existent in our measurement in both black silicon and planar samples. It should appear at around 3.4 eV and has been associated to impact ionization by hot electrons generated through the transition $\Gamma_{25'}$ - Γ_{15} by Kolodinski *et al.* [18] The explanation that we do not see the feature A could be related to base doping (n-type) combined with induced junction (as compared to p-type doping with Kolodinski) and thus the probability for hot electrons is reduced. However, we cannot totally rule out the role of inaccuracies in reflectance measurements, which are usually relatively high for wavelengths below 350 nm. In summary, all the observations in black silicon are similar to the results obtained in planar devices thereby discarding *e.g.* quantum-confinement effects in the black silicon nanostructure tips.

We have shown that EQE values over 100% in black-silicon induced-junction devices can be achieved in the UV. This result is significant, as it has been achieved without applying any extra energy, such as bias voltage. Moreover, the results suggest that there might be still room for further improvement through texture optimization. While the current results can readily have a high impact on the UV-sensor industry, they are promising considering other applications as well, namely, above unity responses could be possible for longer wavelengths too. For instance by applying similar methods, *i.e.* nanostructures and induced junction in lower band gap materials (such as germanium), carrier multiplication should be present and if efficiently harvested, the response and gain in the infrared part of the spectrum would be enhanced. Another important consequence is that the

thermal losses can be reduced considerably, which minimizes thermal noise and the need for cooling in photovoltaic devices. In addition to photodiodes, solar cells could benefit from carrier multiplication if lower bandgap material could be used to efficiently capture the total energy of the photons without suffering from thermal losses. This applies especially to space applications where the intensity of UV radiation is known to be higher.

CONCLUSIONS

In conclusion, we reported certified measurements that demonstrate external quantum efficiency above unity in a black-silicon induced-junction photodiode without external amplification. In particular, we showed EQE values rising up to 132% at 200 nm wavelength. The effect of black silicon was investigated through: i) numerical simulations of the electric field and electrostatic potential in the nanostructure, ii) comparison of IQE to the corresponding planar photodiode, and iii) analysis of features in the internal quantum efficiency spectra. All the results consistently showed that the high performance is based on effective utilization of multiple carrier generation by impact ionization taking place in the nanostructures. The results suggest that utilizing similar concept in lower band gap materials should be relatively straightforward, possibly extending the above unity performance to lower photon energies.

METHODS

Experimental. The structure of our induced-junction photodetectors is shown schematically in figure 1 (inset). The base material is high-resistivity ($> 10 \text{ k}\Omega\text{cm}$) n -type $\langle 100 \rangle$ crystalline silicon. Black silicon, formed through inductively-coupled reactive ion etching (ICP-RIE) at cryogenic temperatures, extends over the whole active area ($\varnothing=5 \text{ mm}$) to ensure minimum device reflectance. The nanotextured active area is covered with a 20 nm thick atomic layer deposited (ALD) Al_2O_3 layer which is responsible for both, minimizing surface recombination and inducing the hole-collecting junction. The large fixed charge in the alumina, $Q_f = -2.5 \times 10^{12} \text{ cm}^{-2}$ [30], combined with a low substrate doping, produces a large space-charge-region extending about $30 \mu\text{m}$ that efficiently collects the photogenerated carriers. Finally, the detectors feature a p^+ ohmic contact ring around the active area and a standard n^+ contact on the back. Further fabrication details can be found elsewhere [26].

Characterization. EQE of the black silicon photodetector was measured by Physikalisch-Technische Bundesanstalt (PTB). The spectral responsivity of the detector was calibrated by comparison with secondary detector standards using a measurement facility consisting of a radiation source, a double-grating monochromator with order-sorting filters and a detector positioning system. The photocurrents of the detector and of the secondary detector standards were measured in photovoltaic mode by using the same current-to-voltage converter and digital voltmeter. The spectral responsivity of the secondary detector standards had previously been calibrated against PTB's primary national detector standards for optical radiant power, the cryogenic electrical substitution radiometers. The relative standard measurement uncertainty of the black silicon photodetector EQE was between 0.1% and 0.4% in the UV range and 0.05% or smaller in the spectral range between 420 nm and 960 nm. The external quantum efficiency (EQE) of the untextured photodetector was measured with a setup where the detector was illuminated with Bentham ILD-D2-QH-24 dual-lamp light source. The lamp was directly coupled to the entrance port of Bentham TMC300_0060 monochromator where the wavelength was selected with 5 nm bandwidth and focused on the detector. The EQE values were calibrated against Newport 818-UV photodetector which had been calibrated using standards traceable to the National Institute of Standards and Technology (NIST). To obtain the internal quantum efficiencies (IQE), reflectance from the untextured and b-Si surface was measured with an integrating sphere based setup (Agilent Cary 5000).

Numerical calculations. Silvaco Atlas semiconductor device simulator was used to simulate the electric field and electrostatic potential inside the black silicon nano-needle. The simulation model consisted of a 200 nm wide and 700 nm high cylindrically symmetric silicon needle, which was conformally covered with 20 nm thick Al_2O_3 film. The silicon doping concentration was set to $2.25 \times 10^{11} \text{ cm}^{-3}$ uniformly everywhere in the needle and fixed charge density of $-2.5 \times 10^{12} \text{ cm}^{-2}$ was applied to all of the interfaces between silicon and Al_2O_3 .

ACKNOWLEDGEMENTS

M. G. acknowledges support from the project ENE2015-74009-JIN of the Spanish Ministry of Economy and Competitiveness (MINECO) and co-funded by the European Regional Development Fund. J. Heinonen, A. Haarahiltunen and M. Juntunen acknowledges financial support from Business Finland. Aalto University authors acknowledge the ATTRACT project funded by the EC under Grant Agreement 777222. The work is related to the Flagship on Photonics Research and Innovation “PREIN” funded by Academy of Finland.

REFERENCES

1. F. Guo, B. Yang, Y. Yuan, Z. Xiao, Q. Dong, Y. Bi, and J. Huang “A nanocomposite ultraviolet photodetector based on interfacial trap-controlled charge injection” *Nat. Nanotechnol.* **7**, 798-802 (2012)
2. T. W. Marin, I. Janik, D. M. Bartels, and D. M. Chipman “Vacuum ultraviolet spectroscopy of the lowest-lying electronic state in subcritical and supercritical water” *Nat. Commun.* **8**, 15435 (2017)
3. T. Larason and Y. Ohno “Calibration and characterization of UV sensors for water disinfection” *Metrologia* **43**, 151-156 (2006)
4. L. A. Jones, R. W. Worobo, and C. D. Smart “UV Light Inactivation of Human and Plant Pathogens in Unfiltered Surface Irrigation Water” *Appl. Environ. Microbiol.* **80**, 849-854 (2014)
5. D.-H. Park, S.-T. Oh, and J.-H. Lim “Development of a UV Index Sensor-Based Portable Measurement Device with the EUVB Ratio of Natural Light” *Sensors* **19**, 754 (2019)
6. Z. Liu and A. K. Kim “Review of Recent Developments in Fire Detection Technologies” *J. Fire Prot. Eng.* **13**, 129-151 (2003)
7. J. Son “UV detectors: status and prospects” *Proc. SPIE* **10727**, 10270F (2018)
8. Hamamatsu Photonics “Si Photodiodes Selection guide” (Hamamatsu 2019)
9. OSI Optoelectronics “UV Enhanced Series Product Datasheet” (OSI Optoelectronics 2019)
10. W. Shockley and H. J. Queisser “Detailed balance limit of efficiency of pn junction solar cells” *J. Appl. Phys.* **32**, 510 (1961)
11. R. C. Alig, S. Bloom, and C. W. Struck “Scattering by ionization and phonon emission in semiconductors” *Phys. Rev. B* **22**, 5565–5582 (1980).
12. F. Scholze, H. Rabus, and G. Ulm “Mean energy required to produce an electron-hole pair in silicon for photon energies between 50 and 1500 eV” *J. Appl. Phys.* **84**, 2926 (1998).
13. F. Scholze, H. Henneken, P. Kuschnerus, H. Rabus, M. Richter, and G. Ulm “Determination of the electron-hole pair creation energy for semiconductors from the spectral responsivity of photodiodes” *Nucl. Instrum. Methods Phys. Res. A* **439**, 208–215 (2000).
14. V. S. Vavilov “On photo-ionization by fast electrons in germanium and silicon” *J. Phys. Chem. Solids* **8**, 223–226 (1959).
15. A. J. Tuzzolino “Quantum efficiency of silicon in the vacuum ultraviolet” *Phys. Rev.* **134**, A205 (1964).
16. O. Christensen “Quantum efficiency of the internal photoelectric effect in silicon and germanium” *J. Appl. Phys.* **47**, 689 (1976).
17. F. J. Wilkinson, A. J. D. Farmer, and J. Geist “The near ultraviolet quantum yield of silicon” *J. Appl. Phys.* **54**, 1172 (1983).
18. S. Kolodinski, J. H. Werner, T. Wittchen, and H. J. Queisser “Quantum efficiencies exceeding unity due to impact ionization in silicon solar cells” *Appl. Phys. Lett.* **63**, 2405 (1993).
19. M. Wolf, R. Brendel, J. H. Werner, and H. J. Queisser “Solar cell efficiency and carrier multiplication in $\text{Si}_{1-x}\text{Ge}_x$ alloys” *J. Appl. Phys.* **83**, 4213 (1998).

20. G. Yamashita, E. Matsubara, M. Nagai, Y. Kanemitsu, and M. Ashida “Intrinsic carrier multiplication efficiency in bulk Si crystals evaluated by optical-pump/terahertz-probe spectroscopy” *Appl. Phys. Lett.* **105**, 231118 (2014).
21. A. J. Nozik “Quantum dot solar cells” *Physica E* **14**, 115–120 (2002).
22. R. D. Schaller, V. M. Agranovich, and V. I. Klimov “High-efficiency carrier multiplication through direct photogeneration of multi-excitons via virtual single-exciton states” *Nat. Phys.* **1**, 189–194 (2005).
23. R. J. Ellingson, M. C. Beard, J. C. Johnson, P. Yu, O. I. Micic, A. J. Nozik, A. Shabaev, and A. L. Efros “Highly Efficient Multiple Exciton Generation in Colloidal PbSe and PbS Quantum Dots” *Nano Lett.* **5**, 865–871 (2005).
24. M. C. Beard, K. P. Knutsen, P. Yu, Joseph M. Luther, Q. Song, W. K. Metzger, R. J. Ellingson, and A. J. Nozik “Multiple exciton generation in colloidal silicon nanocrystals” *Nano Lett.* **7**, 2506–2512 (2007).
25. M. C. Beard, A. G. Midgett, M. C. Hanna, J. M. Luther, B. K. Hughes, and A. J. Nozik “Comparing Multiple Exciton Generation in Quantum Dots To Impact Ionization in Bulk Semiconductors: Implications for Enhancement of Solar Energy Conversion” *Nano Lett.* **10**, 3019–3027 (2010).
26. M. A. Juntunen, J. Heinonen, V. Vähänissi, P. Repo, D. Valluru, and H. Savin “Near-unity quantum efficiency of broadband black silicon photodiodes with an induced junction” *Nat. Photon.* **10**, 777 (2016).
27. B. Hoex, J. J. H. Gielis, M. C. M. van de Sanden, and W. M. M. Kessels, “On the c-Si surface passivation mechanism by the negative-charge-dielectric Al₂O₃” *J. Appl. Phys.* **104**, 113703 (2008).
28. Werner and Smith “Manipulating the negative fixed charge density at the c-Si/ Al₂O₃ interface” *Appl. Phys. Lett.* **104**, 091604 (2014)
29. S. M. Sze “Physics of Semiconductor Devices” John Wiley & Sons USA 1969
30. P. Repo, and H. Savin “Effect of different ALD Al₂O₃ oxidants on the surface passivation of black silicon” *Energy Procedia* **92**, 381–385 (2016).